

Electronic Coherences in Molecules: The Projected Nuclear Quantum Momentum as a Hidden Agent

Evaristo Villaseco Arribas and Neepa T. Maitra

Department of Physics, Rutgers University, Newark 07102, New Jersey USA

(Dated: June 27, 2024)

Electronic coherences are key to understanding and controlling photo-induced molecular transformations. We identify a crucial quantum-mechanical feature of electron-nuclear correlation, the projected nuclear quantum momenta, essential to capture the correct coherence behavior. For simulations, we show that, unlike traditional trajectory-based schemes, exact-factorization-based methods approximate these correlation terms, and correctly capture electronic coherences in a range of situations, including their spatial dependence, an important aspect that influences subsequent electron dynamics and that is becoming accessible in more experiments.

In photo-induced processes, quantum electronic coherences are key factors influencing many molecular processes. They can serve as control knobs in chemical transformations [1–6] and possibly impact photo-synthetic energy flow in biomolecules [7, 8], as well as quantum information science processes [9]. Aside from the practical interest in creating desired products, studying the generation and evolution of these coherences, including both decay and revival, reveals fundamental properties of how correlations between electrons as well as their interplay with nuclei affect dynamics. Experiments can now track how coherences evolve in time with spatial resolution as well [2, 3, 10, 11].

Electronic coherences are usually defined in the Born-Oppenheimer (BO) representation, but nevertheless can be extracted from experiment for the physical reason that away from regions of strong non-adiabatic coupling (NAC), components of the nuclear wavefunction on different BO surfaces evolve independently. The spatially-resolved electronic coherence is defined as [3, 6, 12]

$$\Gamma_{jk}(\underline{\mathbf{R}}, t) = \chi_j^*(\underline{\mathbf{R}}, t)\chi_k(\underline{\mathbf{R}}, t) \quad (1)$$

for $j \neq k$ (and populations $j = k$), where the $\chi_j(\underline{\mathbf{R}}, t)$ are projected nuclear wavefunctions defined via expanding the full molecular wavefunction in the BO basis: $\Psi(\underline{\mathbf{R}}, \underline{\mathbf{r}}, t) = \sum_j \chi_j(\underline{\mathbf{R}}, t)\Phi_{\underline{\mathbf{R}},j}(\underline{\mathbf{r}})$, with $\Phi_{\underline{\mathbf{R}},j}$ eigenstates of the BO Hamiltonian $H_{\text{BO}}|\Phi_{\underline{\mathbf{R}},j}\rangle = E_j^{\text{BO}}|\Phi_{\underline{\mathbf{R}},j}\rangle$ and with variables $\underline{\mathbf{r}}, \underline{\mathbf{R}}$ denoting all electronic and nuclear coordinates, respectively. While recent advances in experimental techniques allow to measure the electronic coherences with sub-Å spatial resolution [2, 10, 11], most experiments instead measure the spatially-averaged coherence [1–6], $\Gamma_{jk}(t) = \int d\underline{\mathbf{R}}\Gamma_{jk}(\underline{\mathbf{R}}, t)$, often referred to as coherence *tout court*.

The electronic coherence thus measures the overlap of the projected wavefunctions, and semiclassical considerations have identified three mechanisms for how this evolves in time, in particular for decoherence (i.e. its decay) [13]: nuclear density overlap decay, pure dephasing, and electronic state transitions. But open questions remain in the nature of the electron-nuclear corre-

lation in influencing coherences, decoherences, and re-coherences (i.e. revivals after decoherence): The semiclassical analyses focus on the spatially-averaged coherence and hold under some assumed wavepacket form and behavior in certain limits [14], so then do these three mechanisms provide a complete picture fully accounting for correlated electron-nuclear dynamics, or are there other terms in the evolution that can play a key role? While the three mechanisms, and their interplay, have been identified in full quantum dynamical simulations [6], how do they explicitly appear in the electron-nuclear equations of motion? Computational challenges in modeling complex molecules mean that mixed quantum-classical (MQC) methods are mostly used, where one propagates an ensemble of classical nuclear trajectories each carrying a set of quantum electronic coefficients determined self-consistently through a prescribed quantum-classical feedback; can we precisely identify which quantum properties of the nuclear system influence the evolution of electronic coherence and need to be approximated in such approaches? The most commonly-used methods, Ehrenfest and surface-hopping [15, 16] are both fundamentally unable to correctly capture coherence, with overcoherence in Ehrenfest and internal inconsistency in surface-hopping [15, 17–19]. Ref. [20] pointed out that the commonly-used, largely *ad hoc*, decoherence corrections are fundamentally flawed in that they act in a state-wise manner while coherence is a state pair-wise property. Further, if an experiment cannot resolve the spatial character in Eq. 1, an inherent signature of correlation, does it matter if the MQC method does not capture it well if it captures the spatial-average well?

Here we show that even when only the spatially-averaged coherence is measured, the underlying spatial-dependence strongly influences the time-dependence (beyond pure dephasing), and that the projected nuclear quantum momenta, $\nabla_\nu|\chi_j|/|\chi_j|$, are key to capture the correct behavior. Thus electron-nuclear correlation terms that go beyond the earlier semiclassical analyses are essential. In MQC simulations, this means

that even in cases where traditional methods yield the correct coherence over the duration of one interaction event, their wrong spatially-resolved coherence leads to poor behavior at longer times. Instead, methods based on the exact factorization (EF) approach [21–25] better approximate these terms and therefore the spatial structure, giving greatly improved predictions, distinguishing between coherence of wavefunctions on parallel surfaces (unlike *ad hoc* decoherence-corrected methods) and gradual decoherence of non-parallel ones (unlike Ehrenfest). While the existing EF-based approximations contain a crucial dependence on the overall nuclear quantum momentum, we identify their neglect of the individually projected quantities as the culprit for not accurately capturing recoherence events in regions of negligible NAC.

Coherences evolve due to population transitions from NACs ($\langle \Phi_{\underline{\mathbf{R}},j} | \nabla_{\nu} \Phi_{\underline{\mathbf{R}},k} \rangle$ and $\langle \Phi_{\underline{\mathbf{R}},j} | \nabla_{\nu}^2 \Phi_{\underline{\mathbf{R}},k} \rangle$), but also away from those regions when more than one BO surface is populated. To avoid conflating effects from NACs, we begin by considering the exact equation of motion for the spatially-resolved coherence in a situation where all NACs are zero:

$$i\partial_t \Gamma_{jk}(\underline{\mathbf{R}}, t) = \Delta E_{kj}(\underline{\mathbf{R}}) \Gamma_{jk}(\underline{\mathbf{R}}, t) + \sum_{\nu} \frac{1}{2M_{\nu}} \left(\chi_k(\underline{\mathbf{R}}, t) \nabla_{\nu}^2 \chi_j^*(\underline{\mathbf{R}}, t) - \chi_j^*(\underline{\mathbf{R}}, t) \nabla_{\nu}^2 \chi_k(\underline{\mathbf{R}}, t) \right) \quad (2)$$

where $\Delta E_{kj}(\underline{\mathbf{R}}) = E_k^{\text{BO}}(\underline{\mathbf{R}}) - E_j^{\text{BO}}(\underline{\mathbf{R}})$ and the sum over ν is a sum over all nuclei. Eq. (S.8) in the Supplementary Material gives the equation including the NACs. Atomic units ($\hbar = m_e = e^2 = 1$) are used throughout this article. The first term on the right of Eq. 2 can be absorbed in a phase, while the evolution of the coherence magnitude depends on the instantaneous curvatures of the BO projected wavefunctions. Instead, when integrated over space, the explicit dependence on these curvatures vanishes, and we find

$$i\partial_t \Gamma_{jk}(t) = \int \Delta E_{kj}(\underline{\mathbf{R}}) \Gamma_{kj}(\underline{\mathbf{R}}, t) d\underline{\mathbf{R}}, \quad (3)$$

that is, the spatially-averaged coherence explicitly depends on the instantaneous relative difference in shape of the BO surfaces weighted by the spatially-resolved coherence. We make two key observations from Eqs. 2–3: First, *without correct spatial dependence of the coherence (a dependence that inherently signifies electron-nuclear correlation), the time-evolution of the spatially-averaged coherence or populations will be wrong.* Second, *for parallel surfaces (no pure dephasing) the spatially-averaged coherence evolves by merely a phase $\Gamma_{jk}(t) = e^{i(E_k - E_j)t} \Gamma_{jk}(0)$, but while its magnitude is constant in time, there is a spatial structure to these quantities that does evolve in time (last two terms of Eq. (2)).*

A deeper understanding of how nuclear motion influences coherences requires to discern local electron-nuclear correlation effects arising from a classical-like treatment of the nuclear motion via an ensemble of trajectories from non-local effects from nuclear wavepacket delocalization. To address this, we turn to the EF, which, unlike Ehrenfest and surface-hopping, allows a formulation of trajectory-based equations defining exact unique forces on the nuclear trajectories when they are treated classically [26–28], and evolution equations for the populations and coherences. In EF, the full molecular wavefunction takes the form of a single correlated product, $\Psi(\underline{\mathbf{r}}, \underline{\mathbf{R}}, t) = \chi(\underline{\mathbf{R}}, t) \Phi_{\underline{\mathbf{R}}}(\underline{\mathbf{r}}, t)$ with $\int |\Phi_{\underline{\mathbf{R}}}(\underline{\mathbf{r}}, t)|^2 d\underline{\mathbf{r}} = 1 \forall \underline{\mathbf{R}}, t$ [29–38]. (See also Supplementary Material for brief details from these works). The EF yields the notion of a unique nuclear wavefunction that satisfies a Hamiltonian evolution and whose modulus and phase give the exact nuclear density and nuclear current-density, $\mathbf{J}_{\nu}(\underline{\mathbf{R}}, t)$, of the molecular wavefunction [35, 36], central concepts to set up an exact trajectory-based approach.

Writing the EF nuclear wavefunction in terms of an amplitude and phase, $\chi(\underline{\mathbf{R}}, t) = e^{iS(\underline{\mathbf{R}}, t)} |\chi(\underline{\mathbf{R}}, t)|$, and likewise for the projected BO wavefunctions, $\chi_k(\underline{\mathbf{R}}, t) = |\chi_k(\underline{\mathbf{R}}, t)| e^{iS_k(\underline{\mathbf{R}}, t)}$, we have, in the limit of negligible NAC, (see Eq. (S.18) in the Supplementary Material for the general case)

$$\partial_t |\Gamma_{jk}(\underline{\mathbf{R}}, t)| = -|\Gamma_{jk}(\underline{\mathbf{R}}, t)| \sum_{\nu} \left\{ \frac{(\nabla_{\nu} - 2\bar{\mathfrak{S}}_{\nu,jk}) \cdot \mathbf{J}_{\nu}}{|\chi|^2} + \sum_n \frac{|C_n|^2}{2M_{\nu}} \left[\left(4\bar{\mathfrak{Q}}_{\nu,jk} - 2\nabla_{\nu} \right) \cdot (\mathbf{f}_{\nu,n} - \mathbf{f}_{\nu,jk}) + 4\mathfrak{S}_{\nu,n} \cdot \mathbf{f}_{\nu,n} \right] \right\} \quad (4)$$

In Eq. 4, all quantities on the right are functions of $\underline{\mathbf{R}}$ and t , an overline indicates the average over j, k ($\bar{g}_{jk} = (g_j + g_k)/2$), and we have defined $\mathbf{f}_{\nu,k} = \nabla_{\nu}(S_k - S)$. Further, we defined the nuclear quantum momentum \mathbf{Q}_{ν} and projected components $\bar{\mathfrak{Q}}_{k,\nu}$ for each state k through

$$\mathbf{Q}_{\nu} = -\frac{\nabla_{\nu} |\chi(\underline{\mathbf{R}}, t)|}{|\chi(\underline{\mathbf{R}}, t)|} \quad \text{and} \quad \bar{\mathfrak{Q}}_{k,\nu}(\underline{\mathbf{R}}, t) = -\frac{\nabla_{\nu} |\chi_k(\underline{\mathbf{R}}, t)|}{|\chi_k(\underline{\mathbf{R}}, t)|} \quad (5)$$

while $\mathfrak{S}_{\nu,k}$ is the “reduced” contribution

$$\mathfrak{S}_{\nu,k}(\underline{\mathbf{R}}, t) = -\frac{\nabla_{\nu} |C_k(\underline{\mathbf{R}}, t)|}{|C_k(\underline{\mathbf{R}}, t)|} = \bar{\mathfrak{Q}}_{\nu,k} - \mathbf{Q}_{\nu} \quad (6)$$

with $C_k(\underline{\mathbf{R}}, t) = \chi_k(\underline{\mathbf{R}}, t)/\chi(\underline{\mathbf{R}}, t)$, which represent coefficients of the conditional electronic wavefunction $\Phi_{\underline{\mathbf{R}}}(\underline{\mathbf{r}}, t)$ when expanded in the BO basis, $\Phi_{\underline{\mathbf{R}}}(\underline{\mathbf{r}}, t) = \sum_n C_n(\underline{\mathbf{R}}, t) \Phi_{\underline{\mathbf{R}},n}(\underline{\mathbf{r}})$.

Our third key observation follows from Eq. (4): While the first term on the right represents a convective contribution to the time-derivative (see more shortly), *both*

the projected quantum momentum $\mathcal{Q}_{\nu,k}$ and the reduced contribution $\mathfrak{S}_{\nu,k}$, play a crucial role in capturing accurate spatially-resolved populations and coherences, when away from NAC regions. The only other term driving (the magnitude of) the coherence or population evolution, $\sum_n |C_n|^2 \nabla_\nu \cdot (\mathbf{f}_{\nu,k} + \mathbf{f}_{\nu,j} - 2\mathbf{f}_{\nu,n}) = \sum_n |C_n|^2 \nabla_\nu^2 (S_k + S_j - 2S_n)$, depends on differences in curvature of the adiabatic phases, which semiclassically relates to the curvatures of the BO surfaces (see more shortly). A fourth key observation is that *in regions where the coherence between two states has locally collapsed to zero, only the terms depending on $\mathfrak{S}_{\nu,n}$ survive to drive time-evolution of the spatially-resolved coherences and populations; thus, this is responsible for coherence effects away from NACs.*

The unique and unambiguous definition of the total nuclear density and and current-density rooted in the EF, allows us to derive an *exact trajectory-based* equation for the populations and coherences from Eq. (4). We represent the nuclear density as a sum over δ -functions (or very narrow Gaussians) centered at a trajectory position $\underline{\mathbf{R}}^{(I)}(t)$

$$|\chi(\underline{\mathbf{R}}, t)|^2 \rightarrow \frac{1}{N_{tr}} \sum_I \delta(\underline{\mathbf{R}} - \underline{\mathbf{R}}^{(I)}(t)) \quad (7)$$

where $\underline{\mathbf{R}}^{(I)}(t)$ satisfy classical Newton's equations [21, 22] with a generalized Lorentz force dependent on $\Phi_{\underline{\mathbf{R}}}$ that drives the nuclear motion [26–28]. The gradient of the phase S becomes $\nabla_\nu S \rightarrow M_\nu \dot{\underline{\mathbf{R}}}(t) - \mathbf{A}$ where \mathbf{A} is the vector potential in the nuclear Hamiltonian (see Supplemental Material), and the time-derivative along the trajectory given by the convective derivative $d/dt = \partial_t + \sum_{\nu} \dot{\underline{\mathbf{R}}}_\nu^{(I)} \cdot \nabla_\nu$. The spatially-resolved and -averaged coherences and populations become trajectory-ensembles:

$$\begin{aligned} \Gamma_{jk}(\underline{\mathbf{R}}, t) &\rightarrow \frac{1}{N_{tr}} \sum_I \delta(\underline{\mathbf{R}} - \underline{\mathbf{R}}^{(I)}(t)) C_j^{(I)*}(t) C_k^{(I)}(t) \\ \Gamma_{jk}(t) &\rightarrow \sum_I C_j^{(I)*}(t) C_k^{(I)}(t) \end{aligned} \quad (8)$$

Then Eq. 4 becomes

$$\begin{aligned} \frac{d|C_j^* C_k|^{(I)}}{dt} &= - \left| C_j^{*(I)} C_k^{(I)} \right| \sum_{\nu,n} \frac{|C_n^{(I)}|^2}{2M_\nu} \\ &\left[\left(4\mathcal{Q}_{\nu,jk}^{(I)} - 2\nabla_\nu \right) \cdot \left(\mathbf{f}_{\nu,l}^{(I)} - \mathbf{f}_{\nu,jk}^{(I)} \right) + 4\mathfrak{S}_{\nu,n}^{(I)} \cdot \mathbf{f}_{\nu,n}^{(I)} \right] \end{aligned} \quad (9)$$

where all are functions of t alone, and we use the shorthand $g^{(I)} = g(\underline{\mathbf{R}}^{(I)}(t))$.

Away from any NAC, Eq. 9 gives the exact equation for the magnitude of the electronic populations and coherences that trajectory-based methods should be aiming for. The full equation including the NACs, and phases, is given in the Supplemental Material (Eq. (S.33–S.35)). The I -dependence gives the spatially-resolved character in the trajectory-picture: while the

electronic populations ($C_j^{*(I)} C_j^{(I)}(t)$) and coherences ($C_j^{*(I)} C_{k \neq j}^{(I)}(t)$) for each individual trajectory evolve in time in the case of parallel surfaces, their sum over trajectories should remain constant in the limit of a large sampling of the initial distribution, analogous to the discussion below Eq. (3). Time-dependence of the individual $C_k^{(I)}(t)$ indicates spatial-dependence in the coefficients, which is crucial in order to get the correct populations and coherences, even when only ensemble-averaged quantities are measurable, as discussed earlier and as we will see explicitly in some examples shortly.

The traditional trajectory-based methods (Ehrenfest, surface-hopping) give strictly zero time-evolution throughout the ensemble when NACs are negligible because they have no non-local quantum momentum terms, and *ad hoc* decoherence corrections to surface-hopping cause spurious decays. Our examples will demonstrate this has drastic consequences for intermediate and long-term coherence and population dynamics. The prime importance of the projected quantum momenta in Eq. 9 is, on the other hand, partially recognized in the EF-based CTMQC method [21, 22], which approximates these terms. Derived from a well-defined series of approximations on the exact electronic and nuclear equations, the resulting CTMQC equations neglect $\mathfrak{S}_{\nu,k}$, effectively approximating $\mathcal{Q}_{\nu,k}$ by $\mathbf{Q}_\nu \forall k, \nu$. We find (again, for negligible NAC)

$$\begin{aligned} \left(\frac{d|C_j^* C_k|}{dt} \right)_{\text{exact}}^{(I)} &= \left(\frac{d|C_j^* C_k|}{dt} \right)_{\text{CTMQC}}^{(I)} + |C_j^{*(I)} C_k^{(I)}| \\ &\sum_{\nu,n} \frac{|C_n^{(I)}|^2}{2M_\nu} \left[\left(4\mathfrak{S}_{\nu,jk}^{(I)} - 2\nabla_\nu \right) \cdot \left(\mathbf{f}_{\nu,n}^{(I)} - \mathbf{f}_{\nu,jk}^{(I)} \right) + 4\mathfrak{S}_{\nu,n}^{(I)} \cdot \mathbf{f}_{\nu,n}^{(I)} \right] \end{aligned} \quad (10)$$

This expression assumes the semiclassical approximation for the gradient of the phase of the electronic coefficients $\mathbf{f}_{\nu,l}^{(I)} = -\int_0^t \nabla_\nu E_l^{(I)} dt$, valid away from NACs [22]. A consequence of CTMQC's neglect of \mathfrak{S} would be spurious population transfer in regions of zero NAC that is however fixed in implementations by modifying the definition of the quantum momentum to enforce no net transfer in these cases [21, 22, 39]. However, another consequence, that is not fixed by this redefinition, is CTMQC's inability to capture recoherence away from NAC regions (see the fourth observation made earlier, and the example shortly).

Our first example is a slight variation on the one-dimensional three-state model of Ref [20], which we name EL20-SAC, consisting of two parallel electronic states that eventually reach a single avoided crossing (SAC) [15], and a third non-parallel state uncoupled to the other two, as shown in the inset of Fig. 1. The Hamiltonian is given in the Supplemental Material. The system is initialized in a 50 : 25 : 25 coherent superposition

of three gaussian nuclear wavepackets with center momentum 40 bohr^{-1} and position -26 bohr . Despite its simplicity, the model illustrates fundamental aspects of electronic coherences. First, their pair-wise nature [20]: coherence between the pair of parallel states should be maintained while coherence between non-parallel states should be lost due to diverging wavepackets. Second, the need to accurately describe the spatially-resolved coherence, as this is key to correctly capture the dynamics even of spatially-averaged quantities, when entering later into the NAC region.

Figure 1 shows the magnitude of the spatially-averaged electronic coherences between the parallel states (upper panel), non-parallel states (middle panel), and population of the first excited state (lowest panel), obtained from Ehrenfest, surface-hopping with energy-based decoherence correction (SHEDC) [40, 41], EF-based CTMQC, EF-based surface-hopping (SHXF) [23, 42], and the exact calculations. Consider first the evolution before the SAC is reached. Because Ehrenfest remains coherent, it the (spatially-averaged) coherence between the parallel surfaces well but fails to capture the decoherence between the non-parallel surfaces, while the opposite is true of SHEDC in which the parallel coherence erroneously decays and the non-parallel decays much too quickly. In contrast, CTMQC does a good job for both coherences. The more approximate SHXF predicts a little too long non-parallel coherence decay time, and the parallel coherence shows some deviation from constant. All methods capture the (trajectory-averaged) populations well at early times. However, once they reach the SAC, only CTMQC is able to reasonably capture the population and coherence dynamics at the right time, albeit with an overestimation, before settling to about the right values after the non-adiabatic event. SHXF gets the trend in the right direction, but the timing and duration of the event is too long. However the traditional methods are completely wrong: SHEDC shows hardly any transfer and completely wrong coherence behavior, and Ehrenfest's population goes in the wrong direction. While not shown here, we note that the thawed Gaussian approach proposed in Ref. [14] would approximate the early behavior well but has no mechanism to include coupling by the NAC.

Why the spatially-averaged electronic quantities are so poor at later times in the traditional methods is revealed by inspecting the spatially-resolved quantities at earlier times, as plotted in Fig. 2. The projected quantum-momentum terms in the equation of motion creates spatial structure in the coherence (also populations, not shown) that is completely missing in the traditional methods, and that nevertheless correctly ensemble-average to zero at times before the SAC is reached. Even if not measured in experiment, the incorrect spatial structure of the coherence in Ehrenfest and SHEDC lead to incorrect ensemble-averaged popu-

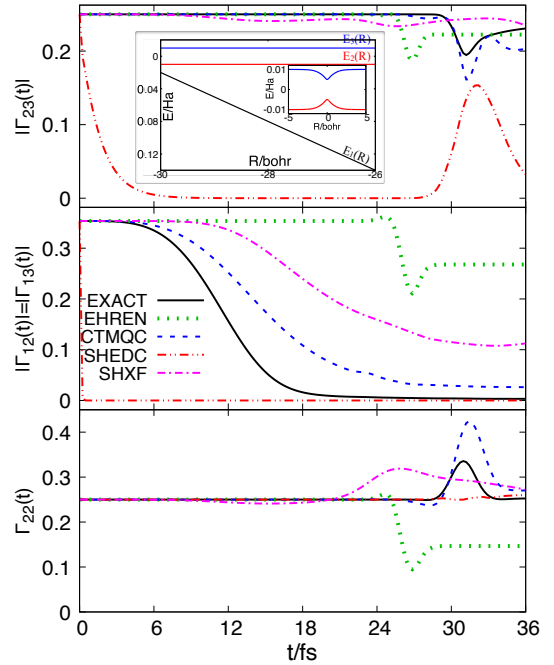


FIG. 1. Electronic state populations of the first excited state (lower panel), and magnitude of electronic coherences between non-parallel (medium panel) and parallel states (upper panel) as a function of time for EL20-SAC model whose adiabatic PES is shown in the inset of the top panel. The NAC is only non-zero in the region of the SAC localized at $R = 0$.

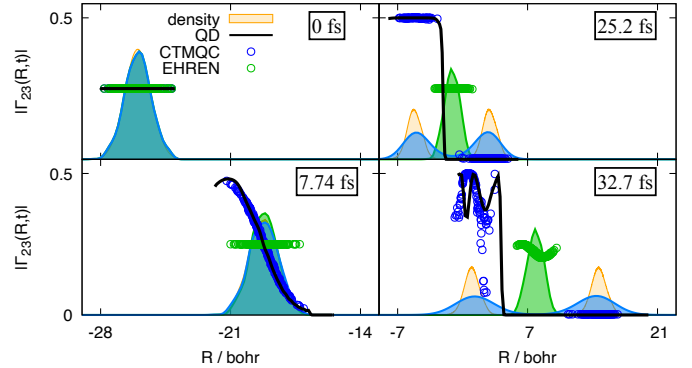


FIG. 2. Time snapshots of the exact density, density reconstructed from the distribution of CTMQC and Ehrenfest trajectories and spatially-resolved electronic coherences between the two parallel surfaces with exact, CTMQC, and Ehrenfest.

lations and coherences at later times, as trajectories enter the SAC with wrong coefficients.

Our second model, denoted 3HO, consists of three uncoupled harmonic oscillators, two of which are parallel (inset of Fig. 3); the Hamiltonian is given in the Supplementary Material. The system is initialized in a $50 : 25 : 25$ coherent superposition of three gaussian nuclear wavepackets with zero momentum centered at -4 bohr . While the wavepackets on the parallel surface maintain

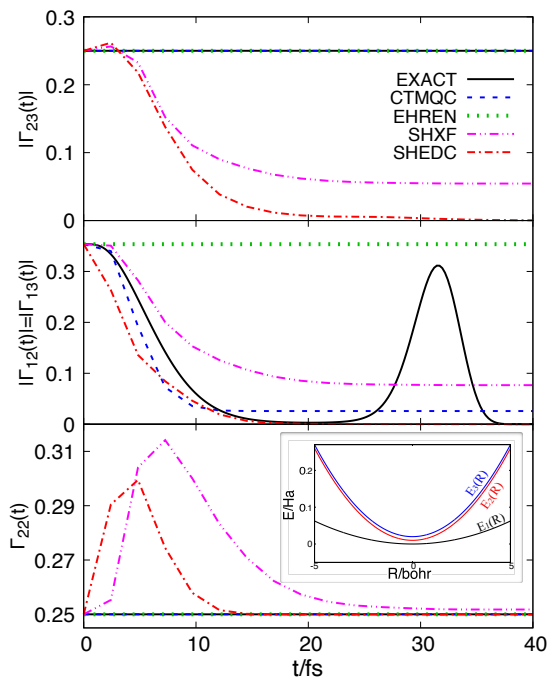


FIG. 3. Electronic state populations of the first excited state (lower panel), and magnitude of electronic coherences between non parallel (medium panel) and parallel states (upper panel) as a function of time for 3HO model. The inset shows the adiabatic PES for 3HO model.

constant coherence, they show successive decoherence and recoherence events with the wavepacket on the non-parallel surface. Figure 3 shows, similar to the EL20-SAC model, that while Ehrenfest maintains coherence between parallel and non parallel states, SHEDC shows decoherence for both. SHXF shows similar behavior to SHEDC, and they both suffer from spurious population transfer [38] as evidenced in the bottom panel. CTMQC on the other hand, shows the correct behavior capturing the first decoherence event while predicting constant spatially-averaged coherences between the parallel surfaces, and correctly constant populations, due its redefinition of the quantum momentum preventing spurious net transfer. However, the recoherence is not well-captured in the EF-based methods, nor in the traditional Ehrenfest and SHEDC, nor would it in the thawed Gaussian approach (not shown here). This is because we enter the domain of the fourth observation made earlier where, after the first decoherence, the \mathfrak{S}_n are the only terms that can drive coherence change, and CTMQC sets this term to zero. The importance of \mathfrak{S}_n is evident from the snapshots of the exact Q , Q_1 and \mathfrak{S}_1 during the first recoherence event shown in the Supplemental Material (Fig. S.1), where \mathfrak{S} displays large features that largely cancel those in Q , crunching it down to yield a relatively small Q_k .

In summary, we have identified the key role played

by the projected nuclear quantum momentum, a signature of electron-nuclear correlation missed in earlier analyses, in determining the correct spatially-resolved electronic coherence, and the importance of the spatial-resolution in influencing the spatially-averaged coherence at later times. The EF approach allows the definition of exact trajectory-based equations for the electronic coefficients, thanks to the notion of a single nuclear wavefunction with the correct density and current-density. Unlike traditional methods, the EF-based CTMQC is promising for simulating electronic coherences in molecules, because it approximates the projected nuclear quantum momentum, and can accurately predict coherences and populations in models in which traditional methods fail miserably, distinguishing coherence between parallel surfaces with and decoherence with non-parallel. Future work will explore a correction to CTMQC that reinstates the neglected \mathfrak{S}_n contribution, which should then be able to capture recoherence, while simultaneously eliminating the need for the redefinition of the quantum momentum in the implementation of that algorithm.

We gratefully acknowledge financial aid from the National Science Foundation Award No. CHE- 2154829, and the Department of Energy, Office of Basic Energy Sciences, Division of Chemical Sciences, Geosciences and Biosciences under Award No. DE-SC0020044, the Computational Chemistry Center: Chemistry in Solution and at Interfaces funded by the U.S. Department of Energy, Office of Science Basic Energy Sciences, under Award No. DE-SC0019394.

-
- [1] B. Kaufman, P. Marquetand, T. Rozgonyi, and T. Weinacht, Long-lived electronic coherences in molecules, *Phys. Rev. Lett.* **131**, 263202 (2023).
 - [2] M. Garg, A. Martin-Jimenez, M. Pizarra, Y. Luo, F. Martín, and K. Kern, Real-space subfemtosecond imaging of quantum electronic coherences in molecules, *Nature Photonics* **16**, 196 (2022).
 - [3] G. Mogol, B. Kaufman, C. Cheng, I. Ben-Itzhak, and T. Weinacht, Direct observation of entangled electronic-nuclear wave packets (2023), arXiv:2311.10588 [quant-ph].
 - [4] V. Despré, N. V. Golubev, and A. I. Kuleff, Charge migration in propiolic acid: A full quantum dynamical study, *Phys. Rev. Lett.* **121**, 203002 (2018).
 - [5] D. Dey, A. I. Kuleff, and G. A. Worth, Quantum interference paves the way for long-lived electronic coherences, *Phys. Rev. Lett.* **129**, 173203 (2022).
 - [6] M. Vacher, M. J. Bearpark, M. A. Robb, and J. a. P. Malhado, Electron dynamics upon ionization of polyatomic molecules: Coupling to quantum nuclear motion and decoherence, *Phys. Rev. Lett.* **118**, 083001 (2017).
 - [7] H. Duan, V. Prokhorenko, R. Cogdell, K. Ashraf, A. Stevens, M. Thorwart, and R. Miller, Nature does not rely on long-lived electronic quantum coherence for

- photosynthetic energy transfer, *Proc. Natl. Acad. Sci.* **114** (2017).
- [8] M. Maiuri, E. E. Ostroumov, R. G. Saer, R. E. Blankenship, and G. D. Scholes, Coherent wavepackets in the fenna–matthews–olson complex are robust to excitonic-structure perturbations caused by mutagenesis, *Nat. Chem.* **10**, 177 (2018).
- [9] M. R. Wasielewski, M. D. E. Forbes, N. L. Frank, K. Kowalski, G. D. Scholes, J. Yuen-Zhou, M. A. Baldo, D. E. Freedman, R. H. Goldsmith, T. Goodson, M. L. Kirk, J. K. McCusker, J. P. Ogilvie, D. A. Shultz, S. Stoll, and K. B. Whaley, Exploiting chemistry and molecular systems for quantum information science, *Nature Reviews Chemistry* **4**, 490 (2020).
- [10] Z. Li, S. Gyawali, A. A. Ischenko, S. Hayes, and R. J. D. Miller, Mapping atomic motions with electrons: Toward the quantum limit to imaging chemistry, *ACS Photonics* **7**, 296 (2020), <https://doi.org/10.1021/acsp Photonics.9b01008>.
- [11] S. Cavaletto, D. Keefer, J. Rouxel, F. Aleotti, F. Segatta, M. Garavelli, and S. Mukamel, Unveiling the spatial distribution of molecular coherences at conical intersections by covariance x-ray diffraction signals, *Proc. Natl. Acad. Sci.* **118** (2021).
- [12] E. Villaseco Arribas, N. T. Maitra, and F. Agostini, Nonadiabatic dynamics with classical trajectories: The problem of an initial coherent superposition of electronic states, *J. Chem. Phys.* **160**, 054102 (2024), <https://pubs.aip.org/aip/jcp/article-pdf/doi/10.1063/5.0186984/19333721/054102.1.5.0186984.pdf>.
- [13] G. A. Fiete and E. J. Heller, Semiclassical theory of coherence and decoherence, *Phys. Rev. A* **68**, 022112 (2003).
- [14] N. V. Golubev, T. Begušić, and J. c. v. Vaniček, On-the-fly ab initio semiclassical evaluation of electronic coherences in polyatomic molecules reveals a simple mechanism of decoherence, *Phys. Rev. Lett.* **125**, 083001 (2020).
- [15] J. C. Tully, Molecular dynamics with electronic transitions, *The Journal of Chemical Physics* **93**, 1061 (1990).
- [16] J. C. Tully, Mixed quantum-classical dynamics, *Faraday Discuss.* **110**, 407 (1998).
- [17] L. Wang, A. Akimov, and O. V. Prezhdo, Recent progress in surface hopping: 2011–2015, *The Journal of Physical Chemistry Letters* **7**, 2100 (2016).
- [18] R. Crespo-Otero and M. Barbatti, Recent advances and perspectives on nonadiabatic mixed quantum–classical dynamics, *Chemical Reviews* **118**, 7026 (2018), pMID: 29767966.
- [19] J. E. Subotnik, A. Jain, B. Landry, A. Petit, W. Ouyang, and N. Bellonzi, Understanding the surface hopping view of electronic transitions and decoherence, *Ann. Rev. Phys. Chem.* **67**, 387 (2016).
- [20] M. P. Esch and B. G. Levine, State-pairwise decoherence times for nonadiabatic dynamics on more than two electronic states, *J. Chem. Phys.* **152**, 234105 (2020).
- [21] S. K. Min, F. Agostini, and E. K. U. Gross, Coupled-Trajectory Quantum-Classical Approach to Electronic Decoherence in Nonadiabatic Processes, *Phys. Rev. Lett.* **115**, 073001 (2015).
- [22] F. Agostini, S. K. Min, A. Abedi, and E. K. U. Gross, Quantum-Classical Nonadiabatic Dynamics: Coupled- vs Independent-Trajectory Methods, *J. Chem. Theory Comput.* **12**, 2127 (2016).
- [23] J.-K. Ha, I. S. Lee, and S. K. Min, Surface Hopping Dynamics beyond Nonadiabatic Couplings for Quantum Coherence, *J. Phys. Chem. Lett.* **9**, 1097 (2018).
- [24] E. Villaseco Arribas and N. T. Maitra, Energy-conserving coupled trajectory mixed quantum-classical dynamics, *J. Chem. Phys.* **158**, 161105 (2023).
- [25] L. Dupuy, A. Rikus, and N. T. Maitra, Exact-factorization-based surface hopping without velocity adjustment, *The Journal of Physical Chemistry Letters* **15**, 2643 (2024).
- [26] C. Li, R. Requist, and E. K. U. Gross, Energy, momentum, and angular momentum transfer between electrons and nuclei, *Phys. Rev. Lett.* **128**, 113001 (2022).
- [27] F. Agostini, A. Abedi, and E. K. U. Gross, Classical nuclear motion coupled to electronic non-adiabatic transitions, *J. Chem. Phys.* **141**, 214101 (2014).
- [28] A. Abedi, F. Agostini, and E. K. U. Gross, Mixed quantum-classical dynamics from the exact decomposition of electron-nuclear motion, *Europhys. Lett.* **106**, 33001 (2014).
- [29] G. Hunter, Conditional probability amplitudes in wave mechanics, *Int. J. Quantum Chem.* **9**, 237 (1975).
- [30] G. Hunter, Ionization potentials and conditional amplitudes, *Int. J. Quantum Chem.* **9**, 311 (1975).
- [31] G. Hunter, Nodeless wave function quantum theory, *Int. J. Quantum Chem.* **9**, 133 (1980).
- [32] G. Hunter, Nodeless wave functions and spiky potentials, *Int. J. Quantum Chem.* **19**, 755 (1981).
- [33] G. Hunter and C. C. Tai, Variational marginal amplitudes, *Int. J. Quantum Chem.* **21**, 1041 (1982).
- [34] N. I. Gidopoulos and E. K. U. Gross, Electronic non-adiabatic states: towards a density functional theory beyond the Born–Oppenheimer approximation, *Philosophical Transactions of the Royal Society of London A: Mathematical, Physical and Engineering Sciences* **372** (2014).
- [35] A. Abedi, N. T. Maitra, and E. K. U. Gross, Exact Factorization of the Time-Dependent Electron-Nuclear Wave Function, *Phys. Rev. Lett.* **105**, 123002 (2010).
- [36] A. Abedi, N. T. Maitra, and E. K. U. Gross, Correlated electron-nuclear dynamics: Exact factorization of the molecular wavefunction, *J. Chem. Phys.* **137**, 22A530 (2012).
- [37] F. Agostini and E. K. U. Gross, Ultrafast dynamics with the exact factorization, *Eur. Phys. J. B* **94**, 179 (2021).
- [38] E. Villaseco Arribas, F. Agostini, and N. T. Maitra, Exact Factorization Adventures: A Promising Approach for Non-Bound States, *Molecules* **27**, 13 (2022).
- [39] S. K. Min, F. Agostini, I. Tavernelli, and E. K. U. Gross, Ab Initio Nonadiabatic Dynamics with Coupled Trajectories: A Rigorous Approach to Quantum (De)Coherence, *J. Phys. Chem. Lett.* **8**, 3048 (2017).
- [40] G. Granucci and M. Persico, Critical appraisal of the fewest switches algorithm for surface hopping, *The Journal of Chemical Physics* **126**, 134114 (2007).
- [41] G. Granucci, M. Persico, and A. Zocante, Including quantum decoherence in surface hopping, *J. Chem. Phys.* **133**, 134111 (2010).
- [42] I. S. Lee, J.-K. Ha, D. Han, T. I. Kim, S. W. Moon, and S. K. Min, PyUNixMD: A Python-based excited state molecular dynamics package, *J. Comput. Chem.* **42**, 1755 (2021).
- [43] F. Agostini, I. Tavernelli, and G. Ciccotti, Nuclear Quantum Effects in Electronic (Non)Adiabatic Dynamics, *Euro. Phys. J. B* **91**, 139 (2018).
- [44] G. A. Worth, M. A. Robb, and I. Burghardt, A novel algorithm for non-adiabatic direct dynamics using variational gaussian wavepackets, *Faraday Discuss.* **127**, 307 (2004).
- [45] M. Ben-Nun and T. J. Martinez, Nonadiabatic molecular

- dynamics: Validation of the multiple spawning method for a multidimensional problem, *J. Chem. Phys.* **108**, 7244 (1998).
- [46] M. Ben-Nun, J. Quenneville, and T. J. Martínez, Ab Initio Multiple Spawning: Photochemistry from First Principles Quantum Molecular Dynamics, *J. Phys. Chem. A* **104**, 5161 (2000).
- [47] D. V. Shalashilin, Quantum mechanics with the basis set guided by Ehrenfest trajectories: Theory and application to spin-boson model, *J. Chem. Phys.* **130**, 244101 (2009).
- [48] D. V. Makhov, C. Symonds, S. Fernandez-Alberti, and D. V. Shalashilin, Ab initio quantum direct dynamics simulations of ultrafast photochemistry with multiconfigurational ehrenfest approach, *Chemical Physics* **493**, 200 (2017).
- [49] D. V. Makhov, W. J. Glover, T. J. Martinez, and D. V. Shalashilin, Ab initio multiple cloning algorithm for quantum nonadiabatic molecular dynamics, *J. Chem. Phys.* **141**, 054110 (2014).
- [50] F. Agostini, E. Marsili, F. Talotta, E. Villasoco Arribas, L. M. Ibele, and E. Sangiogo Gil, G-CTMQC (Last accessed Oct 2023).

SUPPLEMENTARY MATERIAL

SM.1 EXACT FACTORIZATION OF THE MOLECULAR WAVEFUNCTION

The full time-dependent molecular wavefunction can be exactly factorized as a single correlated product [29–38], $\Psi(\underline{\mathbf{r}}, \underline{\mathbf{R}}, t) = \chi(\underline{\mathbf{R}}, t)\Phi_{\underline{\mathbf{R}}}(\underline{\mathbf{r}}, t)$ where the electronic wavefunction satisfies the partial normalization condition $\int |\Phi_{\underline{\mathbf{R}}}(\underline{\mathbf{r}}, t)|^2 d\underline{\mathbf{r}} = 1 \forall \underline{\mathbf{R}}, t$. The marginal factor $\chi(\underline{\mathbf{R}}, t) = e^{iS(\underline{\mathbf{R}}, t)}|\chi(\underline{\mathbf{R}}, t)|$ is interpreted as a nuclear wavefunction because its modulus-square gives the exact nuclear density and the gradient of its phase the exact nuclear current-density (and nuclear velocity field) of the molecular wavefunction:

$$|\chi(\underline{\mathbf{R}}, t)|^2 = \int |\Psi(\underline{\mathbf{r}}, \underline{\mathbf{R}}, t)|^2 d\underline{\mathbf{r}} \quad (\text{S.11})$$

$$\mathbf{V}(\underline{\mathbf{R}}, t) = \frac{\nabla_{\nu} S(\underline{\mathbf{R}}, t)}{M_{\nu}} = \frac{\mathbf{J}_{\nu}(\underline{\mathbf{R}}, t)}{|\chi(\underline{\mathbf{R}}, t)|^2} - \frac{\mathbf{A}_{\nu}(\underline{\mathbf{R}}, t)}{M_{\nu}} \quad (\text{S.12})$$

with $M_{\nu}\mathbf{J}_{\nu}(\underline{\mathbf{R}}, t) = \text{Im}\langle\Psi(\underline{\mathbf{R}}, t)|\nabla_{\nu}\Psi(\underline{\mathbf{R}}, t)\rangle_{\underline{\mathbf{r}}}$. The time-evolution for the electronic and nuclear subsystems satisfy

$$i\partial_t\chi(\underline{\mathbf{R}}, t) = \hat{H}_N(\underline{\mathbf{R}}, t)\chi(\underline{\mathbf{R}}, t) \quad (\text{S.13})$$

$$i\partial_t\Phi_{\underline{\mathbf{R}}}(\underline{\mathbf{r}}, t) = \left[\hat{H}_{el}(\underline{\mathbf{r}}, \underline{\mathbf{R}}) - \epsilon(\underline{\mathbf{R}}, t)\right]\Phi_{\underline{\mathbf{R}}}(\underline{\mathbf{r}}, t) \quad (\text{S.14})$$

The nuclear equation is of Schrödinger form with Hamiltonian

$$\hat{H}_N(\underline{\mathbf{R}}, t) = \sum_{\nu} \frac{(-i\nabla_{\nu} + \mathbf{A}_{\nu}(\underline{\mathbf{R}}, t))^2}{M_{\nu}} + \epsilon(\underline{\mathbf{R}}, t). \quad (\text{S.15})$$

The scalar $\epsilon(\underline{\mathbf{R}}, t) = \langle\Phi_{\underline{\mathbf{R}}}(t)|\hat{H}_{el} - i\partial_t|\Phi_{\underline{\mathbf{R}}}(t)\rangle_{\underline{\mathbf{r}}}$ and vector potentials $\mathbf{A}_{\nu}(\underline{\mathbf{R}}, t) = -i\langle\Phi_{\underline{\mathbf{R}}}(t)|\nabla_{\nu}\Phi_{\underline{\mathbf{R}}}(t)\rangle_{\underline{\mathbf{r}}}$ incorporate the effect of the electronic wavefunction in the nuclear subsystem. On the other hand, the electronic equation is non-linear with electronic Hamiltonian defined as

$$\hat{H}_{el}(\underline{\mathbf{r}}, \underline{\mathbf{R}}) = \hat{H}_{BO}(\underline{\mathbf{r}}; \underline{\mathbf{R}}) + \hat{U}_{eN}[\Phi_{\underline{\mathbf{R}}}, \chi] \quad (\text{S.16})$$

and electron-nuclear coupling operator defined as

$$\hat{U}_{eN} = \sum_{\nu} \frac{1}{M_{\nu}} \left[\frac{(-i\nabla_{\nu} - \mathbf{A}_{\nu}(\underline{\mathbf{R}}, t))^2}{2} + \left(\frac{-i\nabla_{\nu}\chi(\underline{\mathbf{R}}, t)}{\chi(\underline{\mathbf{R}}, t)} + \mathbf{A}_{\nu}(\underline{\mathbf{R}}, t) \right) (-i\nabla_{\nu} - \mathbf{A}_{\nu}(\underline{\mathbf{R}}, t)) \right] \quad (\text{S.17})$$

which incorporates the effect of the nuclear wavefunction in the electronic subsystem.

Note that the factorized form of $\Psi(\underline{\mathbf{r}}, \underline{\mathbf{R}}, t)$ is exact and unique up to a $\underline{\mathbf{R}}$ and t dependent phase, i.e $\tilde{\chi}(\underline{\mathbf{R}}, t) \rightarrow e^{i\theta(\underline{\mathbf{R}}, t)}\chi(\underline{\mathbf{R}}, t)$, $\tilde{\Phi}_{\underline{\mathbf{R}}}(\underline{\mathbf{r}}, t) \rightarrow e^{-i\theta(\underline{\mathbf{R}}, t)}\Phi_{\underline{\mathbf{R}}}(\underline{\mathbf{r}}, t)$, $\tilde{\Psi}(\underline{\mathbf{r}}, \underline{\mathbf{R}}, t) \rightarrow \Psi(\underline{\mathbf{r}}, \underline{\mathbf{R}}, t)$, with $\epsilon(\underline{\mathbf{R}}, t)$ and $\mathbf{A}_{\nu}(\underline{\mathbf{R}}, t)$ transforming according to standard electrodynamic potentials $\tilde{\mathbf{A}}_{\nu}(\underline{\mathbf{R}}, t) \rightarrow \mathbf{A}_{\nu}(\underline{\mathbf{R}}, t) + \nabla_{\nu}\theta(\underline{\mathbf{R}}, t)$ and $\tilde{\epsilon}(\underline{\mathbf{R}}, t) = \epsilon(\underline{\mathbf{R}}, t) + \partial_t\theta(\underline{\mathbf{R}}, t)$.

Although the single-product form of the exact factorization (EF) approach resembles the form of the molecular wavefunction in the Born-Oppenheimer approximation, a significant distinction is that in the former, the equations for the electronic and nuclear wavefunctions must be solved self-consistently, while in the latter, the electronic equation can be solved first for each $\underline{\mathbf{R}}$ and then the nuclear equation solved.

While both the Born-Huang expansion and the exact factorization approach are formally exact, the advantage of using the exact factorization approach for these problems is that it enables the definition of a unique unambiguous force [21, 26–28, 43] that drives nuclear trajectories in mixed quantum-classical (MQC) schemes. This force incorporates coupling to electrons (and any external fields) in a rigorous way. While the Born-Huang expansion also gives a formally exact representation of the molecular wavefunction, it is more challenging to derive a consistent set of equations in MQC schemes because nuclear wavepackets on different electronic surfaces experience different forces, which gives ambiguity to the force on a classical trajectory at a given nuclear position. For example, Ehrenfest simply takes an average of the adiabatic forces, weighted by the electronic coefficients, but this mean-field force cannot yield wavepacket splitting, becoming increasingly unphysical away from regions of strong electron-nuclear coupling (avoided or conical intersections). To avoid this, the surface hopping scheme instead uses an adiabatic

force at all times, but to account for coupling must stochastically hop between active states. While there are more sophisticated trajectory-based schemes stemming from the Born-Huang expansion (e.g. variational multiconfiguration Gaussian [44], ab initio multiple spawning [45, 46], multi-configurational Ehrenfest [47, 48], ab initio multiple cloning [49]), the simplicity and physicality of a single unique nuclear force defined over the ensemble of classical trajectories, with each trajectory associated with quantum electronic coefficients, gives EF-based MQC a particular advantage, conceptually as well as numerically.

SM.2 EXACT EQUATIONS FOR THE EVOLUTION OF ELECTRONIC COHERENCES

The electronic coherence defined in Eq. (1) of the main text, is based on the projected nuclear wavefunctions $\chi_j(\underline{\mathbf{R}}, t)$ in the Born-Huang basis, $\Psi(\underline{\mathbf{r}}, \underline{\mathbf{R}}, t) \stackrel{\text{BO}}{=} \sum_j \chi_j(\underline{\mathbf{R}}, t) \Phi_{\underline{\mathbf{R}}, j}(\underline{\mathbf{r}})$. The full, exact, equation for the time evolution of the magnitude of the electronic coherences of Eq.(1), including non-adiabatic couplings, reads:

$$\begin{aligned} i\partial_t \Gamma_{jk}(\underline{\mathbf{R}}, t) &= \Delta E_{kj}(\underline{\mathbf{R}}) \Gamma_{jk}(\underline{\mathbf{R}}, t) + \sum_{\nu} \frac{1}{2M_{\nu}} \left(\chi_k(\underline{\mathbf{R}}, t) \nabla_{\nu}^2 \chi_j^*(\underline{\mathbf{R}}, t) - \chi_j^*(\underline{\mathbf{R}}, t) \nabla_{\nu}^2 \chi_k(\underline{\mathbf{R}}, t) \right. \\ &\quad - \sum_{n \neq k} [D_{kn, \nu}(\underline{\mathbf{R}}) \Gamma_{jn}(\underline{\mathbf{R}}, t) + 2\chi_j^*(\underline{\mathbf{R}}, t) \mathbf{d}_{kn, \nu}(\underline{\mathbf{R}}) \cdot \nabla_{\nu} \chi_n(\underline{\mathbf{R}}, t)] \\ &\quad \left. + \sum_{n \neq j} [D_{nj, \nu}(\underline{\mathbf{R}}) \Gamma_{nk}(\underline{\mathbf{R}}, t) + 2\chi_k \mathbf{d}_{jn, \nu}(\underline{\mathbf{R}}) \cdot \nabla_{\nu} \chi_n^*(\underline{\mathbf{R}}, t)] \right) \end{aligned} \quad (\text{S.18})$$

where we have assumed real BO states, no geometric phase effects, $\Delta E_{kj} = E_k - E_j$, and where $\mathbf{d}_{nk, \nu}(\underline{\mathbf{R}})$ and $D_{nk, \nu}(\underline{\mathbf{R}})$ are the non-adiabatic coupling vectors $\langle \phi_{\underline{\mathbf{R}}, n} | \nabla_{\nu} \phi_{\underline{\mathbf{R}}, k} \rangle_{\underline{\mathbf{r}}}$ and scalar couplings $\langle \phi_{\underline{\mathbf{R}}, n} | \nabla_{\nu}^2 \phi_{\underline{\mathbf{R}}, k} \rangle_{\underline{\mathbf{r}}}$ respectively. Writing the wavepackets in polar form, i.e $\chi_n(\underline{\mathbf{R}}, t) = |\chi_n(\underline{\mathbf{R}}, t)| e^{iS_n(\underline{\mathbf{R}}, t)}$, we have

$$\nabla_{\nu} \chi_k(\underline{\mathbf{R}}, t) = (i\nabla_{\nu} S_k(\underline{\mathbf{R}}, t) - \mathcal{Q}_{\nu, k}(\underline{\mathbf{R}}, t)) \chi_k(\underline{\mathbf{R}}, t) \quad (\text{S.19})$$

$$\nabla_{\nu}^2 \chi_k(\underline{\mathbf{R}}, t) = (\mathcal{Q}_{\nu, k}(\underline{\mathbf{R}}, t) - 2i\mathcal{Q}_{\nu, k}(\underline{\mathbf{R}}, t) \cdot \nabla_{\nu} S_k(\underline{\mathbf{R}}, t) + i\nabla_{\nu}^2 S_k(\underline{\mathbf{R}}, t) - (\nabla_{\nu} S_k(\underline{\mathbf{R}}, t))^2) \chi_k(\underline{\mathbf{R}}, t) \quad (\text{S.20})$$

where the k-th state projected quantum momentum and quantum potential read

$$\mathcal{Q}_{\nu, k}(\underline{\mathbf{R}}, t) = -\frac{\nabla_{\nu} |\chi_k(\underline{\mathbf{R}}, t)|}{|\chi_k(\underline{\mathbf{R}}, t)|} \quad \text{and} \quad \mathcal{Q}_{\nu, k}(\underline{\mathbf{R}}, t) = \frac{\nabla_{\nu}^2 |\chi_k(\underline{\mathbf{R}}, t)|}{|\chi_k(\underline{\mathbf{R}}, t)|}. \quad (\text{S.21})$$

We now write these quantities in terms of the exact factorization concepts, where we note that

$$\Psi(\underline{\mathbf{r}}, \underline{\mathbf{R}}, t) \stackrel{\text{BO}}{=} \sum_k \chi_k(\underline{\mathbf{R}}, t) \Phi_{\underline{\mathbf{R}}, k}(\underline{\mathbf{r}}) \stackrel{\text{EF}}{=} \chi(\underline{\mathbf{R}}, t) \Phi_{\underline{\mathbf{R}}}^{\text{BO}}(\underline{\mathbf{r}}, t) = \chi(\underline{\mathbf{R}}, t) \sum_k C_k(\underline{\mathbf{R}}, t) \Phi_{\underline{\mathbf{R}}, k}^{\text{BO}}(\underline{\mathbf{r}}) \quad (\text{S.22})$$

where in the last equality the time-dependent conditional electronic wavefunction is represented by its coefficients $\{C_k\}$ in the expansion, which also represent the projected nuclear wavefunction via:

$$\Phi_{\underline{\mathbf{R}}}(\underline{\mathbf{r}}, t) = \sum_k C_k(\underline{\mathbf{R}}, t) \Phi_{\underline{\mathbf{R}}, k}^{\text{BO}}(\underline{\mathbf{r}}) \quad \text{and} \quad \chi_k(\underline{\mathbf{R}}, t) = \chi(\underline{\mathbf{R}}, t) C_k(\underline{\mathbf{R}}, t). \quad (\text{S.23})$$

Writing the nuclear wavefunction χ and the coefficients C_k also in polar form, $\chi(\underline{\mathbf{R}}, t) = |\chi(\underline{\mathbf{R}}, t)| e^{iS(\underline{\mathbf{R}}, t)}$ and $C_k(\underline{\mathbf{R}}, t) = |C_k(\underline{\mathbf{R}}, t)| e^{i\gamma_k}$, Eq. S.23 means we can relate

$$S_k(\underline{\mathbf{R}}, t) = S(\underline{\mathbf{R}}, t) + \gamma_k(\underline{\mathbf{R}}, t) \quad \text{and} \quad |\chi_k(\underline{\mathbf{R}}, t)| = |\chi(\underline{\mathbf{R}}, t)| |C_k(\underline{\mathbf{R}}, t)| \quad (\text{S.24})$$

We define the k-th state reduced quantum momentum as

$$\mathfrak{S}_{\nu, k}(\underline{\mathbf{R}}, t) = -\frac{\nabla_{\nu} |C_k(\underline{\mathbf{R}}, t)|}{|C_k(\underline{\mathbf{R}}, t)|} \quad (\text{S.25})$$

which allows us to write, equivalently to Eq S.19,

$$\nabla_{\nu} C_k(\underline{\mathbf{R}}, t) = (i\nabla_{\nu} \gamma_k(\underline{\mathbf{R}}, t) - \mathfrak{S}_{\nu, k}(\underline{\mathbf{R}}, t)) C_k(\underline{\mathbf{R}}, t) \quad (\text{S.26})$$

Note that the reduced and projected quantum momenta, $\mathfrak{S}_{\nu,k}(\underline{\mathbf{R}}, t)$ and $\mathfrak{Q}_{\nu,k}(\underline{\mathbf{R}}, t)$, are related through the nuclear quantum momentum $\mathbf{Q}_{\nu}(\underline{\mathbf{R}}, t)$

$$\mathbf{Q}_{\nu}(\underline{\mathbf{R}}, t) = -\frac{\nabla_{\nu}|\chi(\underline{\mathbf{R}}, t)|}{|\chi(\underline{\mathbf{R}}, t)|} = \mathfrak{S}_{\nu,k}(\underline{\mathbf{R}}, t) + \mathfrak{Q}_{\nu,k}(\underline{\mathbf{R}}, t) \quad \forall \nu, k \quad (\text{S.27})$$

In terms of these quantities, we write, omitting the dependencies to avoid notational clutter,

$$\begin{aligned} i\partial_t\Gamma_{jk}(\underline{\mathbf{R}}, t) &= \Delta E_{kj}\Gamma_{jk} + \sum_{\nu} \frac{\Gamma_{jk}}{2M_{\nu}} \left(\Delta\mathfrak{Q}_{\nu,jk} + 2i\mathfrak{Q}_{\nu,j}\nabla_{\nu}S_j - i\nabla_{\nu}^2S_j - (\nabla_{\nu}S_j)^2 + 2i\mathfrak{Q}_{\nu,k}\nabla_{\nu}S_k - i\nabla_{\nu}^2S_k + (\nabla_{\nu}S_k)^2 \right) \\ &- \sum_{\nu, n \neq k} \frac{\Gamma_{jn}}{2M_{\nu}} [D_{kn,\nu} + 2i\mathbf{d}_{kn,\nu} \cdot \nabla_{\nu}S_n - 2\mathbf{d}_{kn,\nu} \cdot \mathfrak{Q}_{\nu,n}] + \sum_{\nu, n \neq j} \frac{\Gamma_{nk}}{2M_{\nu}} [D_{nj,\nu} - 2i\mathbf{d}_{jn,\nu} \cdot \nabla_{\nu}S_n - 2\mathbf{d}_{jn,\nu} \cdot \mathfrak{Q}_{\nu,n}] \end{aligned} \quad (\text{S.28})$$

where we define $\Delta g_{jk} = g_j - g_k$ for any quantity. The advantage of writing in terms of exact factorization quantities means we can relate terms to the nuclear density and current-density (with an eventual view towards establishing a mixed quantum-classical method): from Eq. S.12, the inline equation for \mathbf{A}_{ν} below Eq. (S.5), and the expansion in Eq. S.23, we have

$$\nabla_{\nu}S = M_{\nu}\mathbf{V}_{\nu} = \frac{M_{\nu}\mathbf{J}_{\nu}}{|\chi|^2} - \mathbf{A}_{\nu} = \frac{M_{\nu}\mathbf{J}_{\nu}}{|\chi|^2} - \sum_l |C_l|^2 \nabla_{\nu}\gamma_l - \text{Im} \sum_{kl} C_l^* C_k \mathbf{d}_{\nu,lk} \quad (\text{S.29})$$

and

$$\begin{aligned} \nabla_{\nu}^2S &= M_{\nu}\mathbf{J}_{\nu} \cdot \nabla_{\nu} \frac{1}{|\chi|^2} + \frac{M_{\nu}\nabla_{\nu} \cdot \mathbf{J}_{\nu}}{|\chi|^2} - \nabla_{\nu} \cdot \mathbf{A}_{\nu} \\ &= \frac{M_{\nu}}{|\chi|^2} (\nabla_{\nu} \cdot \mathbf{J}_{\nu} + 2(\mathfrak{Q}_{\nu,k} - \mathfrak{S}_{\nu,k}) \cdot \mathbf{J}_{\nu}) - \sum_l |C_l|^2 (\nabla_{\nu}^2\gamma_l - 2\mathfrak{S}_{\nu,l}\nabla_{\nu}\gamma_l) - \text{Im} \nabla_{\nu} \cdot \sum_{kl} C_l^* C_k \mathbf{d}_{\nu,lk} \end{aligned} \quad (\text{S.30})$$

where we wrote $\mathbf{Q}_{\nu} = \mathfrak{Q}_{\nu,k} - \mathfrak{S}_{\nu,k}$ (Eq. (S.27)). In regions where the NACs are zero, this gives

$$\begin{aligned} \partial_t\Gamma_{jk}(\underline{\mathbf{R}}, t) &= -i\Delta E_{kj}(\underline{\mathbf{R}})\Gamma_{jk}(\underline{\mathbf{R}}, t) + \sum_{\nu} \frac{\Gamma_{jk}}{2M_{\nu}} \left[-i\Delta\mathfrak{Q}_{\nu,jk} + 2(\mathfrak{Q}_{\nu,j} + \mathfrak{Q}_{\nu,k}) \cdot \left(\frac{M_{\nu}\mathbf{J}_{\nu}}{|\chi(\underline{\mathbf{R}}, t)|^2} - \sum_l |C_l|^2 \nabla_{\nu}\gamma_l \right) \right. \\ &+ 2(\mathfrak{Q}_{\nu,j} \cdot \nabla_{\nu}\gamma_j + \mathfrak{Q}_{\nu,k} \cdot \nabla_{\nu}\gamma_k) - \frac{2M_{\nu}}{|\chi(\underline{\mathbf{R}}, t)|^2} (\nabla_{\nu} \cdot \mathbf{J}_{\nu} + (\mathfrak{Q}_{\nu,k} + \mathfrak{Q}_{\nu,j} - \mathfrak{S}_{\nu,k} - \mathfrak{S}_{\nu,j}) \cdot \mathbf{J}_{\nu}) \\ &+ 2\sum_l |C_l|^2 (\nabla_{\nu}^2\gamma_l - 2\mathfrak{S}_{\nu,l}\nabla_{\nu}\gamma_l) - \nabla_{\nu}^2(\gamma_k + \gamma_j) - i(\nabla_{\nu}\gamma_k)^2 + i(\nabla_{\nu}\gamma_j)^2 \\ &\left. - 2i\Delta\nabla_{\nu}\gamma_{kj} \cdot \left(\frac{M_{\nu}\mathbf{J}_{\nu}}{|\chi(\underline{\mathbf{R}}, t)|^2} - \sum_l |C_l|^2 \nabla_{\nu}\gamma_l \right) \right] \end{aligned} \quad (\text{S.31})$$

Rearranging and defining $\nabla_{\nu}\gamma_k = \mathbf{f}_{\nu,k}$ we obtain

$$\begin{aligned} \partial_t\Gamma_{jk}(\underline{\mathbf{R}}, t) &= -\Gamma_{jk}(\underline{\mathbf{R}}, t) \left\{ i\Delta E_{kj}(\underline{\mathbf{R}}) + \sum_{\nu} \frac{1}{|\chi|^2} \left[\left(i\Delta\mathbf{f}_{kj} \cdot \mathbf{J}_{\nu} + \nabla_{\nu} \cdot \mathbf{J}_{\nu} - (\mathfrak{S}_{\nu,k} + \mathfrak{S}_{\nu,j}) \cdot \mathbf{J}_{\nu} \right) \right. \right. \\ &+ \sum_{\nu} \frac{1}{2M_{\nu}} \left[i\Delta\mathfrak{Q}_{\nu,jk} + \sum_l |C_l|^2 (2\mathfrak{Q}_{\nu,j} - \nabla_{\nu}) \cdot \Delta\mathbf{f}_{\nu,lj} + \sum_l |C_l|^2 (2\mathfrak{Q}_{\nu,k} - \nabla_{\nu}) \cdot \Delta\mathbf{f}_{\nu,lk} \right. \\ &\left. \left. + 4\sum_l |C_l|^2 \mathfrak{S}_{\nu,l} \cdot \mathbf{f}_{\nu,l} + i\mathbf{f}_{\nu,k}^2 - i\mathbf{f}_{\nu,j}^2 - 2i\Delta\mathbf{f}_{\nu,kj} \cdot \sum_l |C_l|^2 \mathbf{f}_{\nu,l} \right] \right\} \end{aligned} \quad (\text{S.32})$$

(where again $\Delta\mathbf{f}_{\nu,lk} = \mathbf{f}_{\nu,l} - \mathbf{f}_{\nu,k}$). We define $\tilde{\Gamma}_{jk} = \Gamma_{jk} e^{i\int^t \alpha_{jk}(\mathbf{r}, t') dt'}$ where

$$\alpha_{jk}(\underline{\mathbf{R}}, t) = \Delta E_{kj} + \sum_{\nu} \frac{\Delta\mathbf{f}_{kj} \cdot \mathbf{J}_{\nu}}{|\chi|^2} + \sum_{\nu} \frac{1}{2M_{\nu}} \left[\Delta\mathfrak{Q}_{\nu,jk} + \Delta(\mathbf{f}_{\nu,kj}^2) - 2\Delta\mathbf{f}_{\nu,kj} \cdot \sum_l |C_l|^2 \mathbf{f}_{\nu,l} \right] \quad (\text{S.33})$$

such that

$$\partial_t \tilde{\Gamma}_{jk}(\underline{\mathbf{R}}, t) = -\tilde{\Gamma}_{jk} \left\{ \sum_{\nu} \frac{(\nabla_{\nu} - 2\overline{\mathfrak{S}}_{\nu,jk}) \cdot \mathbf{J}_{\nu}}{|\chi|^2} + \sum_{\nu,l} \frac{|C_l|^2}{2M_{\nu}} \left[\overline{(4\mathfrak{Q}_{\nu,jk} - 2\nabla_{\nu}) \cdot (\mathbf{f}_{\nu,l} - \mathbf{f}_{\nu,jk})} + 4\mathfrak{S}_{\nu,l} \cdot \mathbf{f}_{\nu,l} \right] \right\} \quad (\text{S.34})$$

where we use the notation $\overline{g_{jk}} = (g_j + g_k)/2$ to indicate an average over electronic states j and k .

Then, because $\frac{\partial |\Gamma_{jk}|}{\partial t} = 2|\Gamma_{jk}|^2 \text{Re} \left(\frac{1}{\tilde{\Gamma}_{jk}} \frac{\partial \tilde{\Gamma}_{jk}}{\partial t} \right)$, and everything in the curly bracket is real, it follows that Eq. S.34 holds for $\tilde{\Gamma}_{jk}$ replaced by its magnitude, $|\Gamma_{jk}|$, as written in Eq. (4) of the main text. We stress that this is the exact equation for the magnitude of the coherence in the limit of negligible non-adiabatic couplings.

As in the main text, the trajectory-based equation for the populations and coherences follows from these equations by replacing the nuclear density by a sum over delta-functions centered at each member I of the trajectory ensemble

$$|\chi(\underline{\mathbf{R}}, t)|^2 \rightarrow \sum_I^{N_{tr}} (|\chi|^2)^{(I)} = \frac{1}{N_{tr}} \sum_I^{N_{tr}} \delta(\underline{\mathbf{R}} - \underline{\mathbf{R}}^{(I)}(t)) \quad \text{and} \quad (\text{S.35})$$

$$\Gamma_{jk}(\underline{\mathbf{R}}, t) = |\chi(\underline{\mathbf{R}}, t)|^2 C_j^*(\underline{\mathbf{R}}, t) C_k(\underline{\mathbf{R}}, t) \rightarrow \frac{1}{N_{tr}} \sum_I^{N_{tr}} \delta(\underline{\mathbf{R}} - \underline{\mathbf{R}}^{(I)}(t)) C_j^{*(I)}(t) C_k^{(I)}(t) \quad (\text{S.36})$$

and integrating over $\underline{\mathbf{R}}$. The nuclear velocity and the divergence of the current-density become

$$\left. \frac{\mathbf{J}_{\nu}}{|\chi|^2} \right|_{\underline{\mathbf{R}}=\underline{\mathbf{R}}^{(I)}} = \dot{\underline{\mathbf{R}}}_{\nu} \Big|_{\underline{\mathbf{R}}=\underline{\mathbf{R}}^{(I)}} \rightarrow \dot{\underline{\mathbf{R}}}_{\nu}^{(I)} \quad \text{and} \quad \left. \frac{\nabla_{\nu} \cdot \mathbf{J}_{\nu}}{|\chi|^2} \right|_{\underline{\mathbf{R}}=\underline{\mathbf{R}}^{(I)}} = \partial_t \text{Log}(|\chi|^2) \Big|_{\underline{\mathbf{R}}=\underline{\mathbf{R}}^{(I)}} \rightarrow -2\mathbf{Q}_{\nu}^{(I)} \cdot \dot{\underline{\mathbf{R}}}_{\nu}^{(I)} \quad (\text{S.37})$$

where we have invoked the equation of continuity. The trajectory's velocity $\dot{\underline{\mathbf{R}}}_{\nu}^{(I)}$ is given by classical equations of motion derived from the classical nuclear Hamiltonian. Hence, we obtain after integrating Eq. S.32 over $\underline{\mathbf{R}}$

$$\begin{aligned} \partial_t \Gamma_{jk}(t) = & - \sum_I^{N_{tr}} C_j^{(I)*} C_k^{(I)*} \left\{ i\Delta E_{kj}^{(I)} + \sum_{\nu} \left(i\Delta \mathbf{f}_{kj}^{(I)} \cdot \dot{\underline{\mathbf{R}}}_{\nu}^{(I)} - 2\mathbf{Q}_{\nu}^{(I)} \cdot \dot{\underline{\mathbf{R}}}_{\nu}^{(I)} - (\mathfrak{S}_{\nu,k}^{(I)} + \mathfrak{S}_{\nu,j}^{(I)}) \cdot \dot{\underline{\mathbf{R}}}_{\nu}^{(I)} \right) \right. \\ & + \sum_{\nu} \frac{1}{2M_{\nu}} \left[i\Delta \mathfrak{Q}_{\nu,jk}^{(I)} + \sum_l |C_l^{(I)}|^2 (2\mathfrak{Q}_{\nu,j}^{(I)} - \nabla_{\nu}) \cdot \Delta \mathbf{f}_{\nu,lj}^{(I)} + \sum_l |C_l^{(I)}|^2 (2\mathfrak{Q}_{\nu,k}^{(I)} - \nabla_{\nu}) \cdot \Delta \mathbf{f}_{\nu,lk}^{(I)} \right. \\ & \left. \left. + 4 \sum_l |C_l|^2 \mathfrak{S}_{\nu,l}^{(I)} \cdot \mathbf{f}_{\nu,l}^{(I)} + i\mathbf{f}_{\nu,k}^{(I)2} - i\mathbf{f}_{\nu,j}^{(I)2} - 2i\Delta \mathbf{f}_{\nu,kj}^{(I)} \cdot \sum_l |C_l^{(I)}|^2 \mathbf{f}_{\nu,l}^{(I)} \right] \right\} \quad (\text{S.38}) \end{aligned}$$

Further, using the fact that $\overline{\mathfrak{Q}}_{\nu,kj} = \mathbf{Q}_{\nu}^{(I)} - \frac{1}{2}(\mathfrak{S}_{\nu,k}^{(I)} + \mathfrak{S}_{\nu,j}^{(I)})$, we write

$$\begin{aligned} \partial_t \Gamma_{jk}(t) = & - \sum_I^{N_{tr}} C_j^{(I)*} C_k^{(I)*} \left\{ i\Delta E_{kj}^{(I)} + \sum_{\nu} \left(i\Delta \mathbf{f}_{kj}^{(I)} - 2\overline{\mathfrak{Q}}_{\nu,kj} \right) \cdot \dot{\underline{\mathbf{R}}}_{\nu}^{(I)} + \sum_{\nu} \frac{1}{2M_{\nu}} \left[i\Delta \mathfrak{Q}_{\nu,jk}^{(I)} \right. \right. \\ & + \sum_l |C_l^{(I)}|^2 (2\mathfrak{Q}_{\nu,j}^{(I)} - \nabla_{\nu}) \cdot \Delta \mathbf{f}_{\nu,lj}^{(I)} + \sum_l |C_l^{(I)}|^2 (2\mathfrak{Q}_{\nu,k}^{(I)} - \nabla_{\nu}) \cdot \Delta \mathbf{f}_{\nu,lk}^{(I)} \\ & \left. \left. + 4 \sum_l |C_l|^2 \mathfrak{S}_{\nu,l}^{(I)} \cdot \mathbf{f}_{\nu,l}^{(I)} + i\mathbf{f}_{\nu,k}^{(I)2} - i\mathbf{f}_{\nu,j}^{(I)2} - 2i\Delta \mathbf{f}_{\nu,kj}^{(I)} \cdot \sum_l |C_l^{(I)}|^2 \mathbf{f}_{\nu,l}^{(I)} \right] \right\} \quad (\text{S.39}) \end{aligned}$$

We consider the total time-derivative along the trajectory, defined using the convective derivative (Lagrangian frame) $d/dt = \partial_t + \sum_{\mu} \dot{\underline{\mathbf{R}}}_{\mu}^{(I)} \cdot \nabla_{\mu}$. This yields:

$$\frac{d\Gamma_{jk}}{dt} \rightarrow \left(\partial_t + \sum_{\nu} \dot{\underline{\mathbf{R}}}_{\nu} \cdot \nabla_{\nu} \right) \Gamma_{jk} = \partial_t \Gamma_{jk}(t) + \sum_{\nu} \dot{\underline{\mathbf{R}}}_{\nu} \cdot (i\Delta \mathbf{f}_{\nu,kj} - 2\overline{\mathfrak{Q}}_{\nu,kj}) \Gamma_{jk} \quad (\text{S.40})$$

Eq. (S.39) with (S.40) gives the *exact* equation for the coherences for trajectory-based methods in regions of negligible

NAC. Writing in terms of the coefficients (Eq. (S.36)), we obtain

$$\begin{aligned} \sum_I \frac{d(C_j^* C_k)^{(I)}}{dt} &= - \sum_I C_j^{*(I)} C_k^{(I)} \left\{ \sum_{\nu,l} \frac{|C_l|^2}{2M_\nu} \left[\overline{(4\mathcal{Q}_{\nu,jk}^{(I)} - 2\nabla_\nu)} \cdot (\mathbf{f}_{\nu,l}^{(I)} - \mathbf{f}_{\nu,jk}^{(I)}) + 4\mathfrak{S}_{\nu,l}^{(I)} \cdot \mathbf{f}_{\nu,l}^{(I)} \right] \right. \\ &\quad \left. + i\Delta E_{kj}^{(I)} + \sum_\nu \frac{1}{2M_\nu} \left[i\Delta\mathcal{Q}_{\nu,jk}^{(I)} + i\Delta(\mathbf{f}_{\nu,kj}^{(I)})^2 - 2i\Delta\mathbf{f}_{\nu,kj}^{(I)} \cdot \sum_l |C_l^{(I)}|^2 \mathbf{f}_{\nu,l}^{(I)} \right] \right\} \end{aligned} \quad (\text{S.41})$$

Defining $\widetilde{C_j^* C_k}^{(I)} = C_j^{*(I)} C_k^{(I)} e^{i \int (\alpha_{jk} - \sum_\nu \frac{\Delta \mathbf{f}_{kj} \cdot \dot{\mathbf{R}}_\nu}{|\chi|^2}) dt}$ we can write

$$\frac{d(\widetilde{C_j^* C_k})^{(I)}}{dt} = - \widetilde{C_j^* C_k}^{(I)} \left\{ \sum_\nu \frac{1}{2M_\nu} \sum_l |C_l^{(I)}|^2 \left[\overline{(4\mathcal{Q}_{\nu,jk}^{(I)} - 2\nabla_\nu)} \cdot (\mathbf{f}_{\nu,l}^{(I)} - \mathbf{f}_{\nu,jk}^{(I)}) + 4\mathfrak{S}_{\nu,l}^{(\alpha)} \cdot \mathbf{f}_{\nu,l}^{(I)} \right] \right\} \quad (\text{S.42})$$

which by the same argument as given below Eq. S.34 the equation holds for $|C_j^* C_k|^{(I)}$, as given in Eq. 10 of the main text.

Finally, to define the exact trajectory-based propagation equations, we now go back and include the terms from the NAC.

$$\partial_t \Gamma_{jk}(\underline{\mathbf{R}}, t) = \partial_t \Gamma_{jk}(\underline{\mathbf{R}}, t)^{\text{Eq. S.32}} + \partial_t \Gamma_{jk}(\underline{\mathbf{R}}, t)^{\text{NAC}} \quad (\text{S.43})$$

where

$$\begin{aligned} \partial_t \Gamma_{jk}(\underline{\mathbf{R}}, t)^{\text{NAC}} &= - \sum_{\nu, n \neq k} \frac{\Gamma_{jn}}{2M_\nu} \left[-iD_{kn,\nu} + 2\mathbf{d}_{kn,\nu} \cdot \left(\frac{M_\nu \mathbf{J}_\nu}{|\chi|^2} + \sum_l |C_l|^2 \Delta \mathbf{f}_{\nu,nl} + i \sum_{ml} C_l^* C_m \mathbf{d}_{\nu,lm} + i\mathcal{Q}_{\nu,n} \right) \right] \\ &+ \sum_{\nu, n \neq j} \frac{\Gamma_{nk}}{2M_\nu} \left[-iD_{nj,\nu} - 2\mathbf{d}_{jn,\nu} \cdot \left(\frac{M_\nu \mathbf{J}_\nu}{|\chi|^2} + \sum_l |C_l|^2 \Delta \mathbf{f}_{\nu,nl} + i \sum_{ml} C_l^* C_m \mathbf{d}_{\nu,lm} - i\mathcal{Q}_{\nu,n} \right) \right] \\ &+ \sum_\nu \frac{\Gamma_{jk}}{2M_\nu} \left[4i\overline{\mathcal{Q}}_{\nu,jk} \cdot \sum_{lm} C_l^* C_m \mathbf{d}_{\nu,lm} + 2 \sum_{lm} (\Delta \mathbf{f}_{\nu,lm} - 2i\overline{\mathfrak{S}}_{\nu,lm} + i\nabla_\nu) \cdot \mathbf{d}_{\nu,lm} - 2\Delta \mathbf{f}_{\nu,jk} \cdot \sum_{lm} C_l^* C_m \mathbf{d}_{\nu,lm} \right] \end{aligned} \quad (\text{S.44})$$

so that for the trajectory-based coherences and populations, we obtain

$$\sum_I \frac{d(C_j^{*(I)} C_k^{(I)})}{dt} = \sum_I \left(\frac{dC_j^{*(I)} C_k^{(I)}}{dt} \right)^{\text{Eq. S.41}} + \left(\frac{dC_j^{*(I)} C_k^{(I)}}{dt} \right)^{\text{NAC}} \quad (\text{S.45})$$

where

$$\begin{aligned} \left(\frac{dC_j^{*(I)} C_k^{(I)}}{dt} \right)^{\text{NAC}} &= - \sum_{\nu, n \neq k} \frac{(C_j^* C_n)^{(I)}}{2M_\nu} \left[-iD_{kn,\nu}^{(I)} + 2\mathbf{d}_{kn,\nu}^{(I)} \cdot \left(M_\nu \dot{\mathbf{R}}_\nu^{(I)} + \sum_l |C_l^{(I)}|^2 \Delta \mathbf{f}_{\nu,nl}^{(I)} + i \sum_{ml} (C_l^* C_m)^{(I)} \mathbf{d}_{\nu,lm}^{(I)} \right. \right. \\ &\quad \left. \left. + i\mathcal{Q}_{\nu,n}^{(I)} \right) \right] + \sum_{\nu, n \neq j} \frac{(C_n^* C_k)^{(I)}}{2M_\nu} \left[-iD_{nj,\nu}^{(I)} - 2\mathbf{d}_{jn,\nu}^{(I)} \cdot \left(M_\nu \dot{\mathbf{R}}_\nu^{(I)} + \sum_l |C_l^{(I)}|^2 \Delta \mathbf{f}_{\nu,nl}^{(I)} + i \sum_{ml} (C_l^* C_m)^{(I)} \mathbf{d}_{\nu,lm}^{(I)} - i\mathcal{Q}_{\nu,n}^{(I)} \right) \right] \\ &+ \sum_\nu \frac{(C_j^* C_k)^{(I)}}{M_\nu} \sum_{lm} C_l^{*(I)} C_m^{(I)} \left[2i\overline{\mathcal{Q}}_{\nu,jk}^{(I)} + \Delta \mathbf{f}_{\nu,lm}^{(I)} - 2i\overline{\mathfrak{S}}_{\nu,lm}^{(I)} + i\nabla_\nu + \Delta \mathbf{f}_{\nu,kj}^{(I)} \right] \cdot \mathbf{d}_{\nu,lm}^{(I)} \end{aligned} \quad (\text{S.46})$$

SM.3 SIMULATION DETAILS

For the quantum dynamics (QD) simulations, the time-dependent Schrödinger equation is solved on a grid in the diabatic basis using the split-operator method. The system is initialized in a coherent superposition of three gaussian nuclear wavepackets

$$|\Psi(R, 0)\rangle = \chi(R, 0) (|\phi_{R,1}\rangle + |\phi_{R,2}\rangle/2 + |\phi_{R,3}\rangle/2) \quad (\text{S.47})$$

with $\chi(R, 0) = \left(\frac{2\pi^{1/2}}{3\sigma}\right)^{1/2} e^{-\frac{(R-R_0)^2}{2\sigma^2} + i(R-R_0)P_0}$. The initial variance, position, momentum are $(\sigma, R_0, P_0) = (1 \text{ bohr}, -26 \text{ bohr}^{-1}, 40 \text{ bohr})$ for the EL20-SAC model and $(\sigma, R_0, P_0) = (0.223 \text{ bohr}, -4 \text{ bohr}, 0 \text{ bohr}^{-1})$ for the 3HO model. For the EL20-SAC model the spatial grid is defined in the range $[-26 : 28]$ bohr with 4000 grid points and with a time-step of $dt = 0.0012$ fs. For the 3HO model the chosen spatial grid range is $[-10 : 10]$ bohr with 2000 grid points and with a time-step of $dt = 0.0024$ fs.

The trajectory-based simulations were performed in the G-CTMQC package [50] and the SHXF simulations in the PYUNIXMD package [42]. In both models 1000 Wigner-sampled trajectories were run using the same initial conditions as for the exact case. The initial trajectory ensemble for all methods, was initialized in a pure ensemble, i.e each trajectory carries the same coherent superposition of electronic states. The active states for the surface hopping simulations were stochastically selected to match the net populations at the initial time. We refer the reader to Ref. [12] for a study on different choices (pure and mixed) of initial electronic state in trajectory-based methods.

Example 1: EL20-SAC

The Hamiltonian in the diabatic basis is given by

$$H(R) = \begin{pmatrix} V_1(R) & 0 & 0 \\ 0 & V_2(R) & \lambda(R) \\ 0 & \lambda(R) & -V_2(R) \end{pmatrix} \quad (\text{S.48})$$

with

$$\begin{aligned} V_1(R) &= -0.03(R + 35) - 0.02 \\ V_2(R) &= \frac{R}{|R|} A \left(1 - e^{-B|R|}\right) \\ \lambda(R) &= C e^{-DR^2} \end{aligned} \quad (\text{S.49})$$

the chosen model parameters were $A = 0.01 \text{ Ha}$, $B = 1.6 \text{ bohr}^{-1}$, $C = 0.005 \text{ Ha}$ and $D = 1 \text{ bohr}^{-2}$.

Example 2: 3HO

The Hamiltonian reads

$$H(R) = \begin{pmatrix} \frac{1}{2}k_1R^2 & 0 & 0 \\ 0 & \frac{1}{2}k_2R^2 + \Delta & 0 \\ 0 & 0 & \frac{1}{2}k_2R^2 + 2\Delta \end{pmatrix} \quad (\text{S.50})$$

with $k_1 = 0.005 \text{ Ha}^2$, $k_2 = 0.02 \text{ Ha}^2$ and $\Delta = 0.01 \text{ Ha}$.

SM.4 EFFECT OF \mathfrak{S}

To show the importance of $\mathfrak{S}(R, t)$ we plotted time-snapshots of the exact $Q_1(R, t)$, $\mathfrak{S}_1(R, t)$ and $\mathcal{Q}_1(R, t)$ during the first recoherence event. We observe both the nuclear quantum momentum Q_1 and the reduced contribution \mathfrak{S}_1 are active during this event, and the large features that Q_1 displays are offset largely by \mathfrak{S}_1 yielding a relatively small \mathcal{Q}_1 . As discussed in the main text, the \mathfrak{S} terms are responsible to induce recoherence away from NAC regions causing a change in the electronic coherences which then activates the terms dependent on $Q(R, t)$.

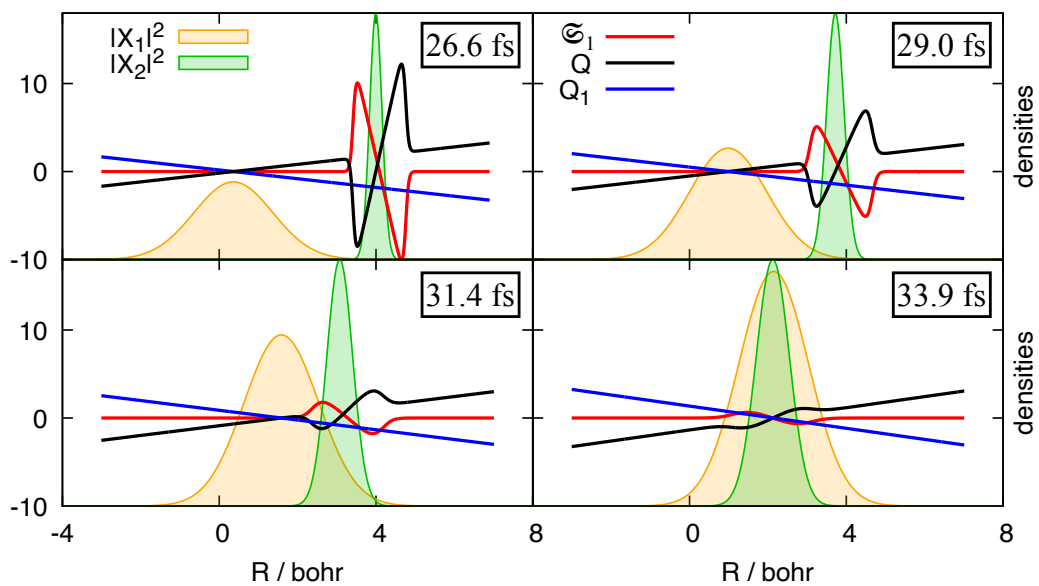


FIG. S.1. Time snapshots of the exact density on the first (orange) and second (green) electronic states, nuclear quantum momentum (blue line), and projected quantum momentum (black line) and crunch term (red line) on state 1 during the recoherence event for 3HO model.